

Metal Nodes of Metal-Organic Frameworks can Activate Molecular Hydrogen

Arianna Melillo,^[a, b] Antonio Franconetti,^[c] Mercedes Alvaro,^[a] Belen Ferrer,^{*[a]} and Hermenegildo Garcia^{*[a, b]}

Abstract: Hydrogenation of multiple bonds are among the most general and important organic reactions. Typical heterogeneous catalysts are based on transition metal nanoparticles, including noble metals. Data are presented here showing that metal nodes of MIL-101(Cr) and UiO-66 in the absence of occluded metal nanoparticles can promote hydro-

genation of polarized X=Y double bonds of nitro and carbonyl groups. The catalytic activity is a function of the composition of the metal node and the organic linker. It is proposed that the reaction mechanism is based on the operation of frustrated Lewis acid/base pairs.

Introduction

Catalytic hydrogenations of multiple bonds are among the most important reactions in organic chemistry from the industrial and synthetic point of view.^[1,2] The reaction can be promoted using a large variety of homogeneous and heterogeneous catalysts.^[3] Among the latter, supported transition metal nanoparticles, including noble metals, but also first row transition metals are the most widely used and deeply studied.^[4] Typical supports for these metal nanoparticles include active carbons, large surface area metal oxides and porous materials.^[5] Metal-organic frameworks (MOFs), constituted by metal nodes coordinated in a precise directionality to rigid organic linkers defining a highly porous crystal lattice, have been also amply studied as supports of occluded metal nanoparticles with a remarkable activity and stability in catalytic hydrogenation.^[6] In these reactions, MOFs play in most of the cases a passive role hosting the catalytically active metal nanoparticle, increasing its catalytic stability by impeding

particle growth due to spatial restrictions imposed by the MOF lattice.^[6] In some cases, a synergy between the metal nanoparticle and the MOF has been observed, due to the cooperation of the adsorption capacity of MOFs and/or tuning the polarity of the internal voids in which the metal nanoparticles are accommodated. However, as far as we know, the active role of MOF lattice, particularly the MOF metal nodes, promoting by themselves hydrogenations has not been disclosed. Intrinsic catalytic hydrogenation activity of MOFs would open a new research aimed at delineating the scope, optimization of the metal/linker combination, deep understanding of the nature of the active sites and determination of the reaction mechanism.

Herein we report that UiO-66 and MIL-101(Cr) in the absence of any metal nanoparticle or any other additional component are able to activate molecular hydrogen promoting hydrogenation of polar X=Y multiple bonds. DFT calculations suggest that metal oxo clusters in MOFs can be active sites of H₂ activation by promoting heterolytic cleavage of the H–H bond. Related to the present study, there are in the literature some reports on the use of isopropanol and other alcohols to perform hydrogen transfer reduction of carbonyl groups by MOFs.^[7,8] This hydrogen transfer mechanism, however, involves hydride transfer of the hydrogen atom at the alpha position of the metal-alcoholate intermediate to the carbonyl group and it is essentially different from the more general direct activation of apolar molecular hydrogen.

Results and Discussion

The six samples under study correspond to two of the most robust MOF structures, namely UiO-66^[9] and MIL-101(Cr),^[10] having large pores and high surface area and they may be taken as exemplary cases for other MOFs. The four materials with UiO-66 structure studied here differ on the composition of the metal node (Zr or Ce or bimetallic Zr–Ce) and the substituent on the linker (terephthalate or aminoterephthalate).

[a] Dr. A. Melillo, Prof. Dr. M. Alvaro, Prof. Dr. B. Ferrer, Prof. H. Garcia
Departamento de Química
Universitat Politècnica de València
Camino de Vera s/n, 46022 Valencia (Spain)
E-mail: hgarcia@qim.upv.es

[b] Dr. A. Melillo, Prof. H. Garcia
Insituto Universitario de Tecnología Química
Consejo Superior de Investigaciones Científicas-Universitat Politècnica de València
av. De los Naranjos s/n, 46022, Valencia (Spain)

[c] Dr. A. Franconetti
CIC BioGUNE
Bizkaia Science and Technology Park
Building 800, 48160 Derio, Bizkaia (Spain)

Supporting information for this article is available on the WWW under <https://doi.org/10.1002/chem.202202625>

© 2022 The Authors. Chemistry - A European Journal published by Wiley-VCH GmbH. This is an open access article under the terms of the Creative Commons Attribution Non-Commercial License, which permits use, distribution and reproduction in any medium, provided the original work is properly cited and is not used for commercial purposes.

Besides showing the general scope of UiO-66 MOFs in H₂ activation, this series allows to address the role of the nodal metal composition and the basicity of the linker. The two MIL-101(Cr) materials having terephthalate or chloroterephthalate as linkers serve to expand the H₂ activation process to other metal-oxo clusters and determine the influence of the ligand inductive effect on the metal node. Table 1 lists the samples studied, their composition and relevant textural parameters, including surface area and pore volume.

All the samples have been previously reported in the literature and were obtained directly from the corresponding metal salts and the corresponding terephthalic acid following reported solvothermal procedures. The samples exhibit the expected XRD diffraction pattern according to their structure (Figure S1 in Supporting Information), FTIR spectra (Figure S1) and the specific surface area is in the range of reported values for these materials (Table 1 and Figure S1), following the trend of lesser area for substituted terephthalate linkers and for Ce UiO-66 in comparison to the Zr analog. These characterization data confirm the successful preparation and the identity of the materials based on their coincidence with the reported values. Other relevant characterization data are collected in the Supporting Information.

Initial catalytic hydrogenation reactions were carried out in acetonitrile solution using nitrobenzene as substrate under 3 bar H₂ pressure. Control experiments in the absence of any catalyst or in the presence of catalyst but in the absence of H₂ only resulted in barely detectable percentages of aniline, lesser than 3%. In contrast to the blank control and unexpectedly according the state of the art, all the samples exhibit hydrogenation activity, aniline being the only product detected in almost complete selectivity. Figure 1 shows the temporal profile of nitrobenzene conversion for some of the MOF catalysts tested. As it can be seen in that Figure, the aniline yield at final reaction times follows the order: UiO-66(Zr/Ce) > MIL-101(Cr)-Cl > MIL-101(Cr) > UiO-66(Zr)-H ≈ UiO-66(Ce)-H > UiO-66(Zr)-NH₂. Inspection of the temporal profiles of nitrobenzene conversion showed, however, that the initial reaction rates do not follow the same order than the final nitrobenzene conversion and that for some MOFs the reaction stops before nitrobenzene conversion was complete. A possible explanation for this behavior is that aniline, as it is being formed during the course of the reaction, acts as a poison of the active sites, slowing down the rate and eventually stopping completely the process. This poisoning effect would be apparently different depending on the MOF.

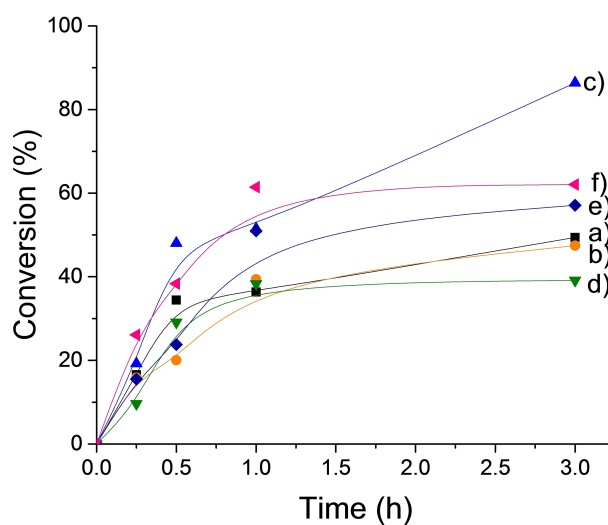
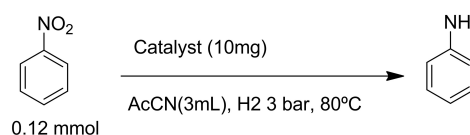


Figure 1. Catalytic nitrobenzene reduction to aniline using UiO-66(Zr)-H (a, black), UiO-66(Ce)-H (b, orange), UiO-66(Zr/Ce)-H (c, blue), UiO-66(Zr)-NH₂ (d, green), MIL-101(Cr)-H (e, dark blue) and MIL-101(Cr)-Cl (f, pink). Reaction conditions: catalyst (10 mg of MOF), nitrobenzene (37 μ L, 0.12 mmol), acetonitrile (3 mL), 80 $^{\circ}$ C, 3 bar H₂. The continuous lines are a guide for the eyes and do not correspond to a fitting to any kinetic model.

To check this possibility, two reactions were performed using UiO-66(Zr)-H under the same conditions, but adding since the beginning aniline at two intermediate concentrations of those formed in the reaction. Measurements of the fresh UiO-66(Zr)-H catalysts in the absence and in the presence of aniline clearly show that the initial reaction rate progressively decreases as the concentration of aniline increases, thus, confirming that aniline is deactivating or blocking the active sites. The results are presented in Figure S1 in the Supporting Information.

The influence of H₂ pressure and the catalyst amount on the hydrogenation activity was determined in the range from 3 to 10 bar using 5 or 10 mg of catalyst. The temporal profiles of nitrobenzene conversion for these experiments using UiO-66(Zr)-H as catalysts are presented in Figure 2. As it can be seen there, the activity increased with the H₂ pressure and with the amount of UiO-66(Zr)-H. A linear relationship between the initial

Table 1. List of MOFs employed as hydrogenation catalysts in this work and their relevant textural and analytical data.

MOF	Zr _{theoretical} /Zr _{experimental} [%]	Ce _{theoretical} /Ce _{experimental} [%]	Cr _{theoretical} /Cr _{experimental} [%]	Pore volume [cm ³ /g]	BET [m ² /g]
UiO66 (Zr)-H	32.8/31.6	–	–	0.8	1258
UiO66 (Ce)-H	–	25.3/21.2	–	0.35	916
UiO66 (Zr/Ce)-H	30.9/22.2	6.5/5.5	–	0.69	1297
UiO66 (Zr)-NH ₂	31.2/30.9	–	–	0.91	923
MIL-101(Cr)-H	–	–	21.7/20	1.44	2690
MIL-101(Cr)-Cl	–	–	18.7/19.52	1.1	1199

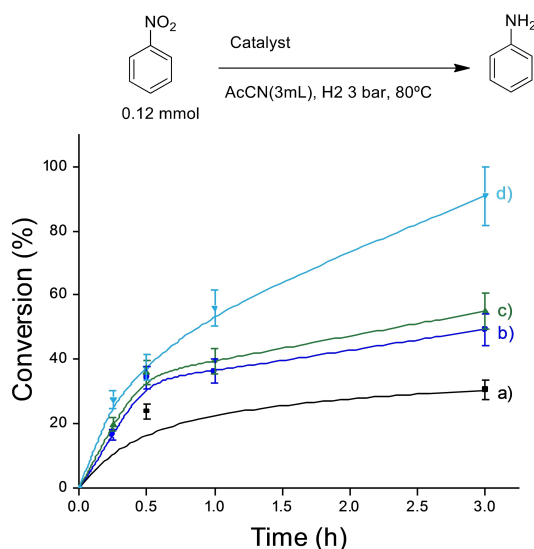


Figure 2. Time-conversion plots of nitrobenzene using UiO-66(Zr)-H in different conditions: a) 5 mg of catalyst, 3 bar of H₂, 80 °C (black); b) 10 mg of catalyst, 3 bar of H₂, 80 °C (blue); c) 10 mg of catalyst, 5 bar of H₂, 80 °C (green); d) 10 mg of catalyst, 10 bar of H₂, 80 °C (light green). Reaction conditions: catalyst (10 mg), nitrobenzene (37 μL, 0.12 mmol), CH₃CN (3 mL).

reaction rate and initial H₂ pressure suggests that the reaction follows a first order kinetics respect to H₂ in the range of pressures under consideration (see Figure S2). Under the best reaction conditions, a conversion of nitrobenzene of 90% was achieved for 10 mg of UiO-66(Zr)-H catalyst after 3 h reaction time. It should be commented at this point that blank controls in the absence of catalysts at increasing H₂ pressure showed

that the uncatalyzed aniline formation increases with the H₂ pressure, but the uncatalyzed nitrobenzene hydrogenation always remained below 10% at 3 h reaction time.

A series of experiments were performed to determine the scope of the catalytic activity. The most commonly studied UiO-66(Zr)-H was used in most of this screening, although the results with nitrobenzene shown in Figure 1 suggest that bimetallic UiO-66(Zr/Ce)-H is even more efficient. Table 2 summarizes the results obtained. In comparison to nitrobenzene, no conversion of 3-nitrostyrene was achieved in 3 h at 3 bar H₂ pressure, even at 130 °C. A 3-nitrostyrene conversion of 77% was, however, achieved at 3 h working at 10 bar H₂ pressure and 80 °C. The only product formed was 3-amino-styrene, indicating that hydrogenation is exquisitely selective for polarized multiple bonds, but no for C=C double bonds. Similar, but lower, selectivity was reported using supported Au NPs as catalysts, since C=C hydrogenation occurred in detectable amounts.^[11] This selectivity towards -NO₂ vs. C=C was again confirmed by checking styrene hydrogenation by UiO-66(Zr)-H, whereby no conversion was observed for 3 h reaction time at 80 °C and 3 bar H₂ pressure.

The relative lesser reactivity of 3-nitrostyrene vs. nitrobenzene can be rationalized considering the hydrogenation reaction is sensitive to the molecular diameter of the substrate. Similar effects have been observed in microporous zeolites and attributed to relative intracrystalline diffusion rates. Thus, the larger molecular diameter of 3-nitrostyrene in comparison to nitrobenzene will disfavor diffusion of the larger substrate inside the MOF pores, making more difficult the approach of the encumbered molecule with the appropriate orientation to the active metal nodes. This geometrical limitation will be less important when higher H₂ pressure will increase the number of

Table 2. Selective hydrogenation of different substrates catalyzed by different materials.

Run	Substrate	Catalyst	H ₂ pressure [bar]	Temperature [°C]	Time [h]	Conversion [%]
1	3-Nitrostyrene	UiO-66(Zr)-H	3	80	3	0
2	3-Nitrostyrene	UiO-66(Zr)-H	3	130	3	0
3	3-Nitrostyrene	UiO-66(Zr)-H	10	80	3	77
4	3-Nitrostyrene	UiO-66(Zr/Ce)-H	3	80	3	51
5	Nitrobenzene	UiO-66(Ce)-H	/	80	6	6
6	Nitrobenzene	UiO-66(Ce)-H	5	80	3	61
7	Nitrobenzene	UiO-66(Ce)-H	10	80	3	76
8	Benzaldehyde	UiO-66(Zr)-H	3	80	3	69
9	<i>P</i> -anisaldehyde	UiO-66(Zr)-H	3	80	3	76
10	<i>Trans</i> -cinnamaldehyde	UiO-66(Zr)-H	3	80	3	0
11	<i>Trans</i> -cinnamaldehyde	UiO-66(Zr)-H	3	100	5	0
12	<i>Trans</i> -cinnamaldehyde	UiO-66(Zr)-H	3	120	5	0
13	<i>Trans</i> -cinnamaldehyde	UiO-66(Zr/Ce)-H	3	80	3	56
14	cyclohexanone	UiO-66(Zr)-H	3	80	24	81
15	<i>i</i> -octanal	UiO-66(Zr)-H	3	80	3	44
16	Cyclooctanone	UiO-66(Zr)-H	3	80	3	40
17	Geranial	UiO-66(Zr)-H	3	80	3	0
18	Geranial	UiO-66(Zr/Ce)-H	3	80	3	0
19	Quinoline	UiO-66(Zr)-H	3	80	3	0
20	Quinoline	UiO-66(Zr/Ce)-H	3	80	3	0
21	Acetophenone	UiO-66(Zr)-H	3	80	3	38
22	Acetophenone	UiO-66(Zr/Ce)-H	3	80	3	57
23	Benzaldehyde + Aniline	UiO-66(Zr)-H	3	80	6	93
24	Benzaldehyde + Aniline	/	3	80	6	0
25	Cyclohexanone oxime	UiO-66(Zr)-H	3	80	3	0
26	Cyclohexanone oxime	UiO-66(Zr/Ce)-H	3	80	3	0
27	Styrene	UiO-66(Zr)-H	3	80	3	0

active sites in UiO-66(Zr)-H probably to less encumbered position. The ability of UiO-66(Zr)-H to catalyze hydrogenation of polar multiple bonds was also tested for benzaldehyde and anisaldehyde at 80 °C. The corresponding benzylic alcohols were formed in both cases about 70%, although benzaldehyde gave somewhat lower yield at 3 h.

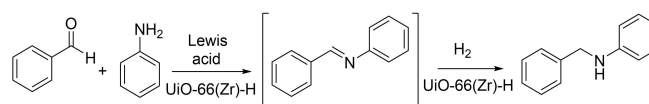
In accordance with size restrictions to pore diffusion and with the lower reactivity of conjugated enals, *trans*-cinnamaldehyde does not undergo reduction under the same conditions. Aliphatic long chain aldehydes, such as octanal, undergo also hydrogenation to the corresponding alcohol, but the yields at 3 h were lower than that of the benzaldehyde, due to the comparative unfavorable diffusion and site approach. In accordance with this rationalization, geranial does not undergo hydrogenation at 3 h under 3 bar H₂ pressure.

Ketone groups can also undergo hydrogenation. Acetophenone can be reduced to 1-phenylethanol, albeit the yields at the same time were lower than those of benzaldehyde probably reflecting the unfavorable combination of steric encumbrance and lesser carbonyl reactivity. Small ketones like cyclohexanone could be reduced in high yields, although the reaction required longer times. Impeded diffusion is also the most likely reason of the lower reactivity of cyclooctanone compared to cyclohexanone.

The overall conclusion of Table 2 is that UiO-66(Zr)-H exhibits an intrinsic activity as hydrogenation catalyst for nitro and carbonyl group, while is not able under the present conditions to promote hydrogenation of C=C double bonds. Product yields appear to depend on the steric encumbrance of the X=Y group. In those cases in which UiO-66(Zr)-H did not give satisfactory yields, further experiments were performed using UiO-66(Zr/Ce)-H that was the most active catalyst in the series. It was observed that 3-nitrostyrene undergoes hydrogenation in the presence of UiO-66(Zr/Ce)-H at 80 °C even at 3 bar H₂ pressure, reaching 51% yield, while UiO-66(Zr)-H was unable to promote hydrogenation under these conditions. Similarly, UiO-66(Zr/Ce)-H was able to promote *trans*-cinnamaldehyde hydrogenation to *trans*-cinnamyl alcohol in 56% with complete selectivity in 3 h at 80 °C. Higher yields of 57% to 1-phenylethanol were also obtained at 3 h and 80 °C using UiO-66(Zr/Ce)-H in comparison with the single metal UiO-66(Zr). However, UiO-66(Zr/Ce)-H also failed as UiO-66(Zr)-H to promote hydrogenation of geranial, cyclohexanone oxime or quinoline, indicating that there is still room for improvement of MOFs as hydrogenation catalysts.

The possibility to use the ability of MOFs to promote hydrogenation, as well as other reactions to develop a tandem reaction was evaluated by carrying out the condensation of aldehyde with primary amines, followed by hydrogenation of the resulting imine to a secondary amine (Scheme 1). The results achieved using benzaldehyde and aniline as starting materials are presented also in Table 2. As it can be seen there, benzaldehyde and aniline afford in the presence of UiO-66(Zr) after 6 h reaction time the expected phenyl benzyl amine in very high yield.

In contrast to the ability of UiO-66(Zr)-H to promote hydrogenation of in situ formed imines, attempts to perform



Scheme 1. Tandem benzaldehyde/aniline condensation and subsequent imine hydrogenation catalyzed by UiO-66(Zr)-H.

hydrogenation of a nitrogenated heterocycle such as quinoline were unsuccessful working at 80 °C and 3 bar H₂ pressure.

Catalyst stability for nitrobenzene hydrogenation was evaluated using UiO-66(Zr)-H as catalyst. At the end of the reaction the solid was recovered, washed with acetonitrile and used in the subsequent run. A gradual catalyst deactivation was observed upon use, the final aniline yield at 3 h reaction time decreasing from 40 to 35 to 25%. Figure S3 in Supporting Information provides the temporal profiles of UiO-66(Zr)-H recycling test. XRD pattern of the three-times used, partially-deactivated UiO-66(Zr)-H showed, however, that the catalyst has preserved the crystallinity. It is proposed that this deactivation derives from the poison effect of aniline that could not be completely removed from the UiO-66(Zr)-H sample after its use as catalysts. However, attempts to reactivate the partially-deactivated UiO-66(Zr)-H catalyst by a more exhaustive washing were unsuccessful, meaning that some fraction of aniline remains interacting strongly with the active sites.

To gain some evidence of H₂ activation by UiO-66(Zr)-H, in situ IR spectra were acquired after exposure of UiO-66(Zr)-H to H₂ gas at 60 °C Figure 3 shows illustrative IR spectra of these measurements. After evacuation, the IR spectrum of pristine UiO-66(Zr)-H shows a broad O–H stretching vibration band from 3600 till 2500 cm⁻¹. This spectrum did not change with time. Exposure of this evacuated UiO-66(Zr)-H sample in the cell

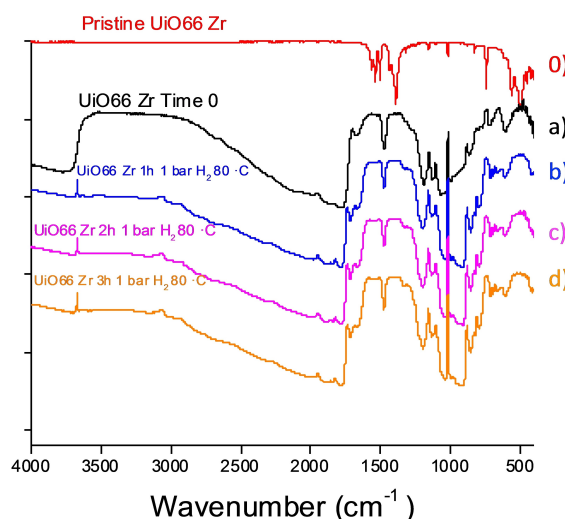
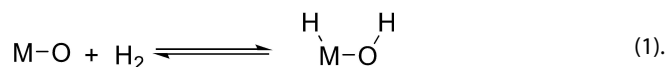


Figure 3. FTIR spectra after adsorbing H₂ on UiO66(Zr)-H (a), UiO66(Zr)-H after 1 h at 80 °C (b), UiO66(Zr)-H after 2 h at 80 °C (c) and UiO66(Zr)-H after 3 h at 80 °C (d) or pristine UiO66 (Zr)-H (0). The peak at 3670 cm⁻¹ is associated to the generation of the O–H that correspond to the protonation of a nodal O atom.

chamber to H₂ at atmospheric pressure shows the appearance of a sharp O–H stretching peak at about 3600 cm⁻¹. The wavenumber and narrow width of the peak indicates that they correspond to isolated OH that do not form hydrogen bridges. However, appearance of other peaks was not observed. It is proposed that the generation of the O–H peak should correspond to protonation of a nodal O atom and it would be accompanied by the formation of Zr–H. However, the position of this proposed Zr–H would appear at about 1600 cm⁻¹[12] and would be overlapped with the intense MOF lattice vibrations, being difficult to detect.

Thus, based on the observation of the formation of O–H the following equation for H₂ chemisorption on UiO-66(Zr)-H is proposed in Equation (1). There are precedents in the literature providing evidence of heterolytic H–H bond cleavage in metal oxides



DFT calculations

Aimed at understanding the interaction of H₂ and substrate with the UiO-66 nodes as a function of the metal ion substitution, Density Functional Theory (DFT) calculations were carried out to determine the electron density and strength of the interaction of H₂ with three UiO-66 models at M11-L/def2-SVP level of theory. Exchange of Zr⁴⁺ by Ce⁴⁺ can modify H₂ adsorption and reactivity ending up in a modulation of the catalytic activity. Metal ion-oxide interfaces are involved in two different processes: (a) *substrate binding* and (b) *H₂ dissociation* and subsequent hydrogen spillover. Since our experimental data indicate a first-order kinetics respect to H₂, its dissociation process should be key for the catalytic activity. As an initial hypothesis, our models assume the presence of one linker defect that should create unsaturated coordination positions at the metal centers (Zr⁴⁺ or Ce⁴⁺ ions). In this situation, these metal sites display Lewis acidity.

Substrate binding to these UiO-66 node models was considered in first place. The location of feasible adsorption sites was carried out by analysis of Molecular Electrostatic Potential (MEP) surfaces (Figure 4a) which is a good estimate to account for adsorption processes governed by electrostatic forces. Preliminary checks showed that fully coordinated metal nodes do not provide any site for nitrobenzene adsorption. Therefore, it seems to be clear that linker defects are necessary to enable the adsorption of different adsorbates on the UiO-66 surface as indicated earlier. In general, the introduction of a mixed metal node such as Zr–Ce has a significant influence on the V_s values of the MEP on the metal center, whereas the bridging μ₃-O nodes are almost insensitive (–8 kcal mol⁻¹). In quantitative terms, the V_s value significantly decreases ca. 10 kcal mol⁻¹ for Zr sites and contrarily, V_s values for Ce sites increase, thus tuning the adsorption properties of the nodes and modulating the H₂ splitting.

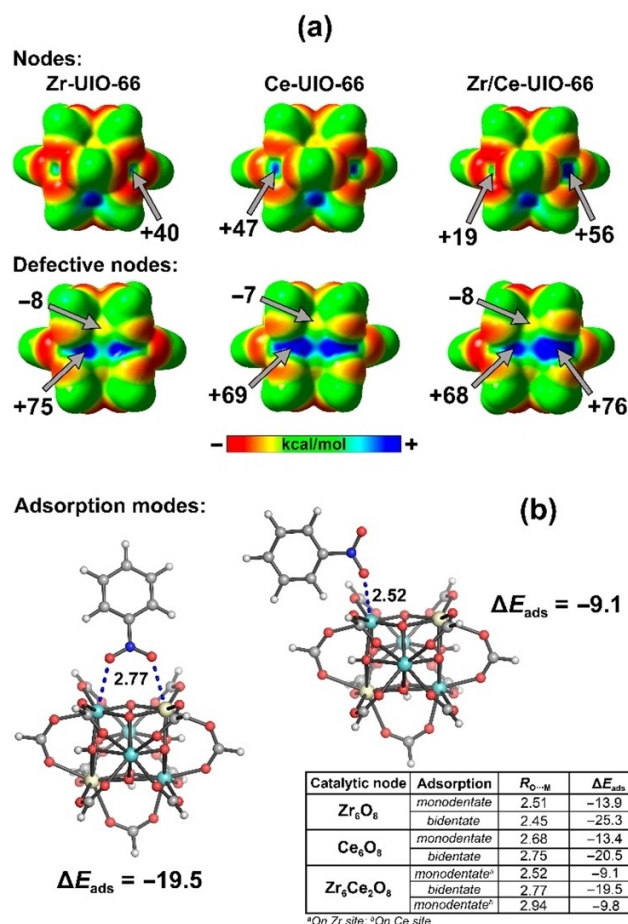


Figure 4. (a) Molecular electrostatic potential (MEP) plotted onto the 0.001 a.u. surface for native Zr, Ce and mixed nodes and unsaturated catalytic sites; (b) Adsorption modes (*monodentate* and *bidentate* coordination) for nitrobenzene. The Table shows the calculated E_{ads} for each catalytic node at M11-L/def2-SVP level of theory. Energies are given in kcal mol⁻¹ and distances in Å. Zr atoms are displayed in light blue and Ce atoms in light yellow.

Adsorption of nitrobenzene was studied taking into account both mono- and bidentate coordination modes. In all cases, the calculated values for E_{ads} (from –9.1 to –25.3 kcal mol⁻¹) are consistent with a physisorption process. As expected, the bidentate coordination is more stable than the monodentate one due to the larger number of interactions. However, bidentate coordination type does not allow the simultaneous co-adsorption of H₂ and nitrobenzene in the model. For this reason, we have focused on the monodentate interaction. The inspection of E_{ads} values reveal that the adsorption in mixed Zr₄Ce₂O₈ catalyst is slightly stronger for Ce-based sites than Zr nodes (Figure 4b, Table). Based on E_{ads} values, the adsorption of aniline is even stronger than nitrobenzene in the range –11.4 to –16.9 kcal mol⁻¹ which may explain the poisoning of the catalyst active sites as experimentally observed.

Hydrogen activation was subsequently studied. Upon the formation of the corresponding vacancy, the proposed mechanism for H₂ activation consists in the heterolytic H–H bond cleavage on the metal node. As a result of this dissociation, the

formation of a hydride-proton pair is proposed. However, different activation pathways are possible depending on the H⁺ migration and its final location onto groups that do not have the capability to dissociate H₂ themselves (terminal –OH at adjacent Zr site or μ_3 -O species).^[13]

Our DFT calculations suggest that the most favorable pathway is the heterolytic cleavage involving an unsaturated metal site with defective linker and the adjacent μ_3 -O group. Firstly, the energetic profile shows that the H₂ adsorption is dependent on the metal (Zr or Ce) active site. For Zr-based systems, this adsorption is preferred on the mixed *Zr₄Ce₂O₈ nodes ($\Delta\Delta G = -0.5$ kcal mol⁻¹) than the Zr₆O₈-based catalyst, as shown in Figure 5. Similarly, the same trend was calculated for H₂ physisorption involving Ce active sites. For these nodes, an additional stabilization of 0.4 kcal mol⁻¹ was calculated for mixed Zr₄*Ce₂O₈ in comparison to the Ce₆O₈ system.

Overall, the H₂ activation is an endergonic process. However, the use of mixed catalytic nodes (Zr₄Ce₂O₈) decreases the activation barrier (ΔG^\ddagger) by 1.6 kcal mol⁻¹. It is noteworthy that the migration started almost simultaneously ($R_{\text{H}\cdots\text{H}} = 1.06$ Å) with the hydrogen dissociation. Stationary points (i.e., transition

states and energy minima) found by scanning the H–H bond breaking suggest a late transition state in agreement with previous reports.^[13] This was further confirmed by topological analysis of electron density through Bader's theory "atoms-in-molecules". The transition states display a bond path connecting the activated H^{δ+}...H^{δ-} moieties with a bond length in the range of 1.29–1.25 Å. The values of electron density, $\rho(r)$, at the bond critical point (CP) are 0.0766 and 0.0839 a.u. for Zr₆O₈ and Zr₄Ce₂O₈, respectively. Larger $\rho(r)$ values at the two additional metal...H and μ_3 -O...H CPs indicate that these contacts, structurally close to dissociation products, are dominant in the transition states. These products are thermodynamically unfavorable (35.7 and 32.7 kcal mol⁻¹ for Zr₆O₈ and Zr₄Ce₂O₈, respectively). Importantly, this heterolytic pathway has low backward energy barriers which enable the reverse reaction. Between the models, the mixed Zr₄Ce₂O₈ node affords a larger barrier ($\Delta G^\ddagger_r = 6.1$ kcal mol⁻¹) than Zr₆O₈ ($\Delta G^\ddagger_r = 4.7$ kcal mol⁻¹) and Ce₆O₈ nodes, in agreement with the experimental trend. At this point, the feasibility of a second transfer from Zr to the adjacent μ_3 -O atom similar to other metal oxide surfaces^[14–15] was also explored. However, the relative free energy calculated for this product indicates that the second H transfer is largely unfavorable ($\Delta G = 74.0$ kcal mol⁻¹), and therefore, this pathway was discarded.

Finally, the ability to accommodate the substrate upon H₂ dissociation was evaluated by the analyses of MEP surfaces. In all cases the V_s values above the adjacent catalytic sites (Zr or Ce) still remain unchanged thus allowing the subsequent substrate coadsorption. Altogether these data support the higher activity of mixed-metal nodes on H₂ activation and tuning substrate binding.

Conclusions

The results presented here show that certain structurally most robust MOFs such as UiO-66 and MIL-101(Cr) have intrinsic sites able to activate molecular H₂ and promote selective hydrogenation reactions of polar X=Y multiple bonds of organic substrates in the absence of any guest. In this way, nitro aromatics and carbonyl groups of aromatic and aliphatic aldehydes and ketones undergo hydrogenation catalyzed by MOFs. Hydrogenation of –NO₂ and C=O is selective in the presence of conjugated C=C double bonds. MOF-promoted hydrogenation can be a part of a tandem reaction. The performance depends on the composition of the MOF, being possible to optimize the activity by appropriate selection of the metal nodes and linkers. One of the key factors controlling the MOF activity is the strong adsorption of the corresponding products that can act as poisons, explaining the progressive deactivation of the MOF catalyst during the course of the reaction and upon reuse. DFT calculations indicate that H₂ adsorption on the nodes occurs at linker-defective metal ions. Hydrogen heterolytic dissociation is an endothermic process that in the case of UiO-66 depends on the metals involved, bimetallic Zr/Ce being predicted the most efficient site compared to monometallic Zr or Ce models. The metal-hydride

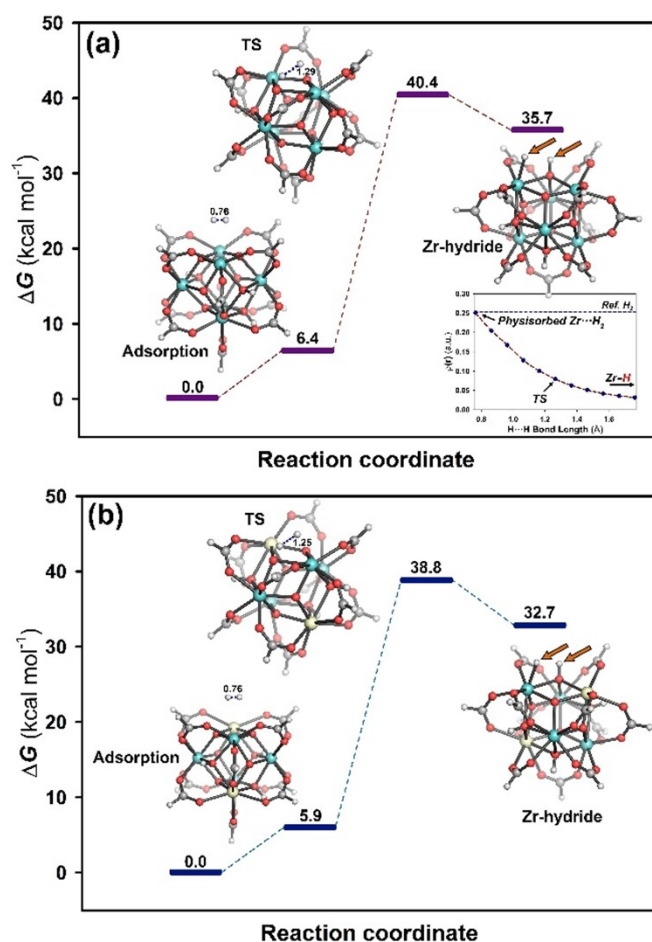


Figure 5. DFT-computed relative free-energy profile for the H₂ adsorption and dissociation at M11-L/def2-SVP level: (a) Zr₆O₈ node. The inset shows the variation of $\rho(r)$ with the H–H bond length; (b) the mixed Zr₄Ce₂O₈ node. Energies are given in kcal mol⁻¹ and distances in Å. Orange arrows indicate the Zr–H and OH species upon dissociation.

character of the intermedia could explain the selectivity toward polar X=Y bonds. Considering the flexibility offered by MOFs in the selection of transition metal and linkers, including multi-metallic structures, the present finding opens a new avenue for the synthesis of purposely designed MOFs as hydrogenation catalysts for multiple bonds the target being the delineation of the functional groups that can be activated and substrate scope.

Experimental Section

All reagents used for the synthesis of the materials and for the catalytic reactions were purchased from Sigma Aldrich and are used without additional purification.

Synthesis of UiO66-(Zr)-H: The synthesis of Zr-BDC MOF was carried out dissolving the metallic precursor $ZrCl_4$ (0.053 g, 0.227 mmol) and the organic linker 1,4-benzenedicarboxylic acid (H_2BDC) (0.034 g, 0.227 mmol) in *N,N'*-dimethylformamide (DMF) (24.9 g, 340 mmol) at room temperature. The transparent suspension was transferred in a Teflon-lined autoclave, sealed and placed in a pre-heated oven at 220 °C for 12 h. The resulting white solid formed after this time was filtered and washed several times with DMF and methanol and later, dried at room temperature.

For the synthesis of the other MOFs of the series, characterization techniques and details of the DFT calculation see the Supporting Information.

Catalytic activity: The catalytic activity of UiO-66(X, X: Zr, Ce or Zr/Ce)-Y (Y: H or NH_2) and MIL-101(Cr)-L (L: H or Cl) was tested introducing the required catalyst amount (5 or 10 mg) into a 10 mL Pyrex tube reactor containing a pressure gauge at the outlet and a gas inlet. Then, the specific reagent (0.12 mmol) was dissolved in acetonitrile (3 mL), and the suspension containing MOF, was subjected to ultrasound for 20 min. Subsequently, the system was purged with H_2 for 15 min and, then, pressurized to the selected value for each reaction. The reaction was heated at different temperatures. The course of the reaction was followed by gas chromatography, analyzing diluted reaction aliquots (0.1 mL) in acetonitrile (0.5 mL) introducing a known amount of nitrotoluene as internal standard. Prior to analyzed the suspension, the mixture was filtered using a nylon filter (0.2 μm).

Acknowledgements

Financial support by the Spanish Ministry of Science and Innovation (Severo Ochoa and PDI2021-126071-OB-CO21) and Generalitat Valenciana (Prometeo 2021-083) are gratefully

acknowledged. Authors also thank the Galicia Supercomputing Centre (CESGA) for computational facilities.

Conflict of Interest

The authors declare no conflict of interest.

Data Availability Statement

The data that support the findings of this study are available from the corresponding author upon reasonable request.

Keywords: catalytic hydrogenation · heterogeneous catalysis · metal-organic frameworks as catalysts · UiO-66 as hydrogenation catalyst

- [1] M. A. Stoffels, F. J. Klauk, T. Hamadi, F. Glorius, J. Leker, *Adv. Synth. Catal.* **2020**, *362*, 1258–1274.
- [2] W. Carruthers, I. Coldham, *Some modern methods of organic synthesis*, Cambridge University Press, **1986**.
- [3] S. Nishimura, *Handbook of heterogeneous catalytic hydrogenation for organic synthesis*, Wiley New York, **2001**.
- [4] D. Astruc, *Nanopart. Cat.* **2008**, *16*, 1–48.
- [5] M. J. Ndolomingo, N. Bingwa, R. Meijboom, *J. Mater. Sci.* **2020**, *55*, 6195–6241.
- [6] A. Dhakshinamoorthy, H. Garcia, *Chem. Soc. Rev.* **2012**, *41*, 5262–5284.
- [7] Rojas-S. Buzo, P. García-García, A. Corma, *ChemSusChem* **2018**, *11*, 432–438.
- [8] A. H. Valekar, K.-H. Cho, S. K. Chitale, D.-Y. Hong, G.-Y. Cha, U.-H. Lee, D. W. Hwang, C. Serre, J.-S. Chang, Y. K. Hwang, *Green Chem.* **2016**, *18*, 4542–4552.
- [9] M. Kandiah, M. H. Nilsen, S. Usseglio, S. Jakobsen, U. Olsbye, M. Tilset, C. Larabi, E. A. Quadrelli, F. Bonino, K. P. Lillerud, *Chem. Mater.* **2010**, *22*, 6632–6640.
- [10] M. Latroche, S. Surblé, C. Serre, C. Mellot-Draznieks, P. L. Llewellyn, J. H. Lee, J. S. Chang, S. H. Jung, G. Férey, *Angew. Chem. Int. Ed.* **2006**, *118*, 8407–8411.
- [11] A. Corma, P. Serna, *Science* **2006**, *313*, 332–334.
- [12] B. V. Lokshin, Z. S. Klemenkova, M. G. Ezernitskaya, L. I. Strunkina, E. M. Brainina, *J. Organomet. Chem.* **1982**, *235*, 69–75.
- [13] K. E. Hicks, A. S. Rosen, Z. H. Syed, R. Q. Snurr, O. K. Farha, J. M. Notestein, *ACS Catal.* **2020**, *10*, 14959–14970.
- [14] M. García-Melchor, N. López, *J. Phys. Chem. C.* **2014**, *118*, 10921–10926.
- [15] B. Wei, F. Tielens, M. Calatayud, *Nanomaterials* **2019**, *9*, 1199.

Manuscript received: August 23, 2022

Accepted manuscript online: September 24, 2022

Version of record online: November 7, 2022